RSC Advances

PAPER

View Article Online
View Journal | View Issue

Cite this: *RSC Adv.*, 2023, **13**, 14461

One-pot hydrothermal synthesis of a carbon quantum dot/$CaFe_2O_4$ hybrid nanocomposite for carcinogenic Congo red dye degradation

Muhammad Innam ur Rahman,[a] Hasan M. Khan, *[ab] Muhammad Naeem Ashiq,*[c] Misbah Ul Islam,[a] Saeed Ahmad Buzdar,[a] Imran Sadiq,[g] Shehla Honey,[f] Zahida Batool,[a] Rizwan Sheikh,[d] Muhammad Zahid,[a] Mohammad A. Assiri,[e] Muhammad Imran[e] and Thamraa Alshahrani[h]

Received 16th January 2023
Accepted 26th March 2023

DOI: 10.1039/d3ra00334e

rsc.li/rsc-advances

Semiconductor materials show a restricted degradation response to organic pollutants due to limited photocatalytic activity under visible light. Therefore, researchers have devoted much attention to novel and effective nanocomposite materials. For the first time, herein, a novel nano-sized semiconductor calcium ferrite modified by carbon quantum dots ($CaFe_2O_4$/CQDs) photocatalyst is fabricated *via* simple hydrothermal treatment for the degradation of aromatic dye using a visible light source. The crystalline nature, structure, morphology, and optical parameters of each of the synthesized materials were investigated using X-ray diffraction spectroscopy (XRD), Fourier transform infrared spectroscopy (FT-IR), scanning electron microscopy (SEM), and UV-visible spectroscopy. The nanocomposite exhibits excellent photocatalytic performance (90% degradation) against Congo red (CR) dye. In addition, a mechanism for $CaFe_2O_4$/CQDs improving photocatalytic performance has been proposed. The CQDs in the $CaFe_2O_4$/CQD nanocomposite are considered to act as an electron pool and transporter, as well as a strong energy transfer material, during photocatalysis. $CaFe_2O_4$/CQDs appear to be a promising and cost-effective nanocomposite for dye-contaminated water purification, according to the findings of this study.

1. Introduction

Natural resources like portable water have been directly affected by the explosive increase in organic dyes over the last few decades due to effluents from metal, pharmaceutical, cosmetic and agricultural industries, as well as paper and textile industries.[1–3] Organic synthetic dyes are among the most common pollutants, contributing up to 0.7 million tons of annual global production. In all, existing dyes have a content of 50–70% azo dyes with double bonds (–N=N–) and the phenyl of naphthyl groups that maintain the color of textile fabrics and other materials.[4–6] There are various types of azo dye, monoazo dyes such as methylene blue and methylene orange, diazo dyes such as direct lake blue and Congo red, and direct black BN, which is a poly-azo dye. All of these dyes are used in printing, textiles, pigment, and paints.[6–8] Moreover, azo dye is a hazardous pollutant, and on decomposition, it produces aromatic amines and various secondary by-products that potentially cause mutation, toxicity, allergic reactions and carcinogenic effects. Scientists have subsequently been searching for ways to remove this lethal pollutant from water that represents a serious threat to human health and the environment.[9,10]

Several methods have been employed to reduce high dye concentrations in industrial effluents, including adsorption,[11,12] flocculation, chemical oxidation, electrochemistry and membrane filtration processes.[13–17] All types of physiochemical processes have limitations due to the incomplete removal of organic dyes, and their being time-consuming and high cost.[18] Besides these benefits, photocatalysis has attracted a lot of attention because of its outstanding merits, such as economic efficiency, stability, and ability to degrade a wide range of contaminants. It is generally believed that the photodegradation mechanism of azo dyes destroys azo groups by the oxidation and reduction process of photogenerated holes and electrons.[19] Moreover, the degradation of azo dye through photocatalysis efficiently and rapidly remains a problem due to

---

[a] Institute of Physics, The Islamia University of Bahawalpur, 63100, Pakistan. E-mail: hmkhan@iub.edu.pk
[b] Institute of Physics, Bahauddin Zakaria University, Multan, 60800, Pakistan
[c] Institute of Chemical Sciences, Bahauddin Zakaria University, Multan, 60800, Pakistan. E-mail: naeembzu@bzu.edu.pk
[d] Department of Chemical Engineering, NFC-Institute of Engineering and Technology, Multan, Pakistan
[e] Department of Chemistry, Faculty of Science, King Khalid University, P.O. Box 9004, Abha 61413, Saudi Arabia
[f] Department of Physics, University of Okara, Okara, Pakistan
[g] Centre of Excellence in Solid State Physics, University of Punjab, Lahore, Pakistan
[h] Department of Physics, College of Sciences, Princess Nourah bint Abdulrahman University (PNU), P.O. Box 84428, Riyadh 11671, Saudi Arabia

inadequate utilization of light and high recombination between electrons and holes in the photocatalytic degradation of organic dyes.[20] The above problem has been altered for clarity by constructing a heterojunction between the separated electrons and holes.[21]

One of the demands for mankind is the development of materials that effectively illuminate organic dyes for a sustainable environment.[22] Oxide-based metal photocatalysts have been developed by scientists, and they are fixed on spinal ferrites because of their high stability, enriched visible light conservation, reasonable bandgaps (approximately 1.75 eV), magnetic properties, and controllable optical properties by replacing Fe^{2+} with extra divalent ions.[23,24] However, due to slow migration of the charge carriers and rapid recombination of electrons and holes, the photocatalytic process was not satisfactory. It is possible to reduce this limitation of metal ferrites by constructing a heterostructure of ferrite with a semiconductor. Researchers improved the remarkable photocatalytic efficiency of metal ferrites with carbon dots. For a few decades, a large number of ferrite composites such as $ZnFe_2O_4$, $CoFe_2O_4$-carbon quantum dots,[25] carbon dots/$ZnFe_2O_4$, $BaFe_2O_4$/quantum dots, $CuFe_2O_4/Ti_3C_2$, and zinc tungsten oxide/nickel ferrite[26–28] have been applied as photocatalysts for the degradation of toxic dye. However, Z. Jiang *et al.* reported that the synthesis of an $MgFe_2O_4$/conjugated polyvinyl chloride nanocomposite for the treatment of Cr(VI)-polluted water exhibited higher efficiency under visible light.[29] Kiani *et al.* studied an $MgFe_2O_4$–$MgTiO_3$ nanocomposite which exhibited higher photocatalytic efficiency when employed for the mineralization of organic dyes such as acid black and acid brown dyes under visible light.[30] Shakir *et al.* reported that the fabrication of an $Mn_{0.9}Cu_{0.1}Fe_2O_4$/rGO nanocomposite exhibited a 77% photocatalytic degradation rate of methylene blue (MB) under exposure to visible light irradiation.[31] Xiao *et al.* reported that the chemical synthesis of an $SnFe_2O_4/BiFeO_3$ nanocomposite as a photocatalyst exhibited 100% efficiency for the mineralization of malachite green dye in 60 min under visible light irradiation.[32] Hammouche *et al.* studied the photocatalytic efficiency of undoped and nickel-doped zinc ferrite ($ZnFe_{2-x}Ni_xO_4$) nanocomposites showing 98% efficiency for the degradation of methylene blue (MB) under exposure to visible light irradiation in 58 min, synthesized through a hydrothermal approach.[33] Within 1 h, Abraham *et al.* synthesized zirconium ferrite doped for use in the mineralization of several organic pollutants, including organic dyes (methyl orange, methylene blue, methyl orange, and acid red 18), tetracycline, and pesticides (acephate and 2,4-dichlorophenoxyacetic acid).[34]

Here, we present a facile one-pot hydrothermal synthesis of a $CaFe_2O_4$/CQD nanocomposite that is highly efficient, economical, and stable. The synthesized nanostructures were characterized *via* different techniques to confirm the structure, morphology, and optical properties. The main aims of this work are: (1) the development of a novel binary carbon quantum dots/$CaFe_2O_4$ nanocomposite, (2) the study of its physical, chemical and structural properties, and (3) determination of the potential of nanomaterials for organic dyes.

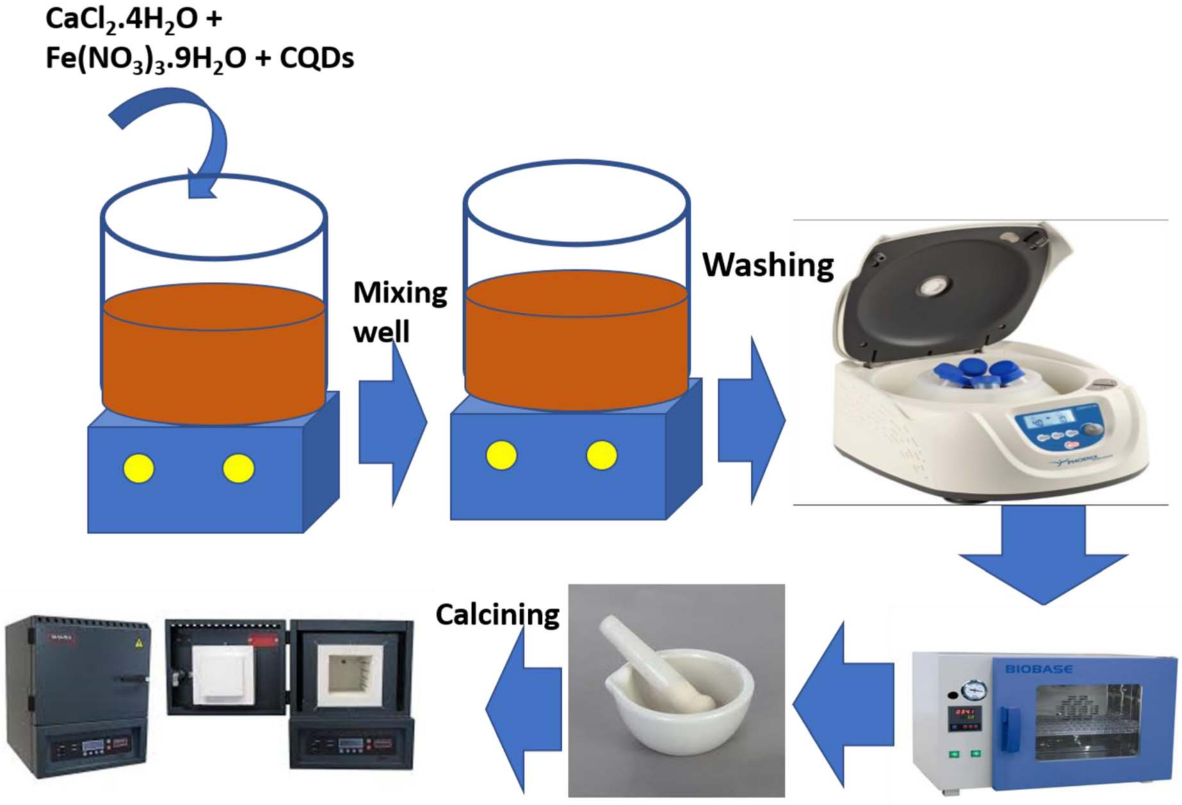

Fig. 1 Schematic synthesis of the $CaFe_2O_4$/CQD nanocomposite.

2. Experimental

2.1 Synthesis of CQDs

CQDs were fabricated *via* a one-step hydrothermal treatment, as previously reported by Wu.[35] L-ascorbic acid (1.62 g), glycol (15 mL), and ultra-pure water (25 mL) were dissolved to form a mixture. To obtain homogeneity, the mixture was magnetically stirred for 30 min, transferred to a 100 mL Teflon-lined autoclave and then heated at 180 °C for 90 minutes. The autoclave was naturally cooled to room temperature, and a yellowish solution was found. The formed product was separated and filtered with an ultra-filtration membrane (0.25 μm) to eliminate side products and particles of huge size. Finally, a yellowish solution comprising CQDs was saved (Fig. 1).

2.2 Synthesis of $CaFe_2O_4$/CQDs

In a typical fabrication procedure, 0.88 g of calcium chloride dihydrate ($CaCl_2 \cdot 2H_2O$) and 4.845 g of iron nitrate nanohydrate ($Fe(NO_3)_3 \cdot 9H_2O$) were dissolved in 30 mL of ultra-pure water under magnetic stirring until a consistent solution was obtained. pH up to 12 was attained using sodium hydroxide (NaOH) in 4 g of solution. The dark brown paste obtained and the already-prepared yellowish CQD solution were shifted into a 100 mL Teflon-lined autoclave and heated at 180 °C for 12 h. Then, the autoclave was naturally cooled to room temperature. Finally, the samples were washed three times with deionized water and once with ethanol before drying at 70 °C overnight. After drying, the sample was ground for 30 min and then employed for calcination at 800 °C for 12 h and then allowed to cool at room temperature. The synthesis scheme for composite formation is depicted in Fig. 1. Simple $CaFe_2O_4$ nanoparticles were also fabricated for comparison purposes.

2.3 Photodegradation performance

A UV-visible spectrophotometer was used to analyze dye degradation in aqueous media using the synthesized photocatalysts, such as $CaFe_2O_4$ and $CaFe_2O_4$/CQDs. Congo red (CR) was utilized as an organic pollutant in this study for degradation under visible light. The powder semiconductor nanocomposite (0.1 g) was added to 100 mL of 10 ppm dye solution. Under visible light irradiation, the resulting reaction mixture was placed in homemade photo reactor (200 W tungsten lamp). The light source was 8 cm away from the beaker containing the mixture. To achieve adsorption–desorption equilibrium, the mixture was constantly agitated in a dark chamber for 30 min. The test suspension was then exposed to visible light to begin the decomposition process. After equal intervals of 0, 20, 40, 60, 80, 100, 120 or 140 min, 5 mL of the mixture was removed and centrifuged to separate the dispersed catalyst. The clear solution was used for UV-visible spectroscopy (Shimadzu UV-2550). Eqn (1) was used to compute the percentage degradation:

$$\text{Degradation (\%)} = C_0 - C/C_0 \times 100 \tag{1}$$

C_0 denotes the initial concentration of the dye solution, while C denotes the concentration of the dye solution at a regular time interval (t).

3. Physical characterization

The prepared sample was analyzed by X-ray diffraction (XRD) using a Bruker D8 Advance Diffractometer (Cu K: = 1.5407: 2θ = 20–80°, 1.5° per min scanning rate: 40 kV/35 mA) to investigate the structural and phase identification. Chemical bonding and functional analysis were studied using a Fourier infrared spectrometer (Bruker Tensor 27) in the 400–4000 cm^{-1} range. Scanning electron microscopy (SEM, FEI Nova NanoSEM 450) was used to examine the surface morphology of the synthesized sample. A Cary 60 Agilent (UV-vis spectrophotometer in the range 200–800 nm) was used to examine optical parameter qualities.

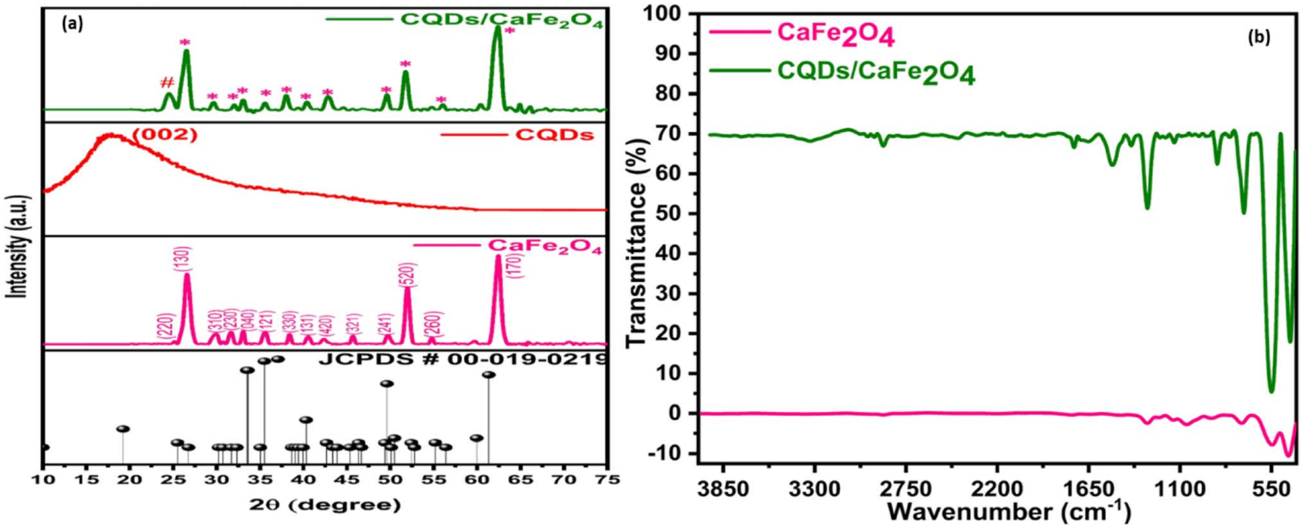

Fig. 2 (a) XRD spectra and (b) FTIR spectra of as-synthesized catalysts.

4. Results and discussion

4.1 X-ray diffraction (XRD)

XRD was used to characterize the phase structure of $CaFe_2O_4$ and $CaFe_2O_4$/CQDs, as shown in Fig. 2(a). The Miller indices (220), (130), (310), (230), (040), (121), (330), (131), (420), (321), (241), (520), (260), and (170) give a reflection of $CaFe_2O_4$ (JCPDS No. 00-019-0219) corresponding to the peaks at 25.7°, 26.9°, 30.5°, 31.8°, 33.5°, 35.6°, 38.7°, 40.4°, 42.8°, 45.5°, 49.4°, 52.6°, 55.9°, and 61.4°, respectively, confirming the orthorhombic phase with *Pnam* space group. The distinct and sharp peaks indicate great purity and crystallinity of the produced products, with no extra peaks of dopant or impurity, indicating successful $CaFe_2O_4$ synthesis. However, in the $CaFe_2O_4$/CQDs, the addition of a single typical peak of CQDs at about 26° can be seen, which could be due to the low content and large dispersion of CQDs in the sample. For the $CaFe_2O_4$/CQDs nanocomposite, the positions of the $CaFe_2O_4$ diffraction peaks remain identical, showing that the introduction of CQDs during synthesis had no effect on the phase structure of $CaFe_2O_4$.

The Scherrer equation:

$$L = \frac{K\lambda}{\beta \cos\theta} \tag{2}$$

4.2 Fourier transform infrared spectroscopy

When a molecule absorbs infrared radiation, chemical bonds vibrate. These are malleable and flexible connections. FTIR spectra of hydrothermally synthesized nanoparticles were determined to be in the 4500–500 cm^{-1} range at ambient temperature, as shown in Fig. 2(b). Between 3096 and 3505 cm^{-1} (the O–H group stretching mode), there is a broad absorption peak.[36] The peaks at 1286 and 1502 cm^{-1} of this spectrum show stretching of the C–O bond.[37] The creation of hydrogen bonds between water and silanol groups triggered this. The absorption peaks 2877 and 2958 cm^{-1} were found to be lower due to weaker stretching of C–H bonds. $CaFe_2O_4$ nanoparticle spectra at 410 and 534 cm^{-1} show Ca–O and Fe–O bonding, respectively.[38] The 862.98 cm^{-1} peak was formed by bending of the Fe–O–H bond,[39] whereas the 709.80 cm^{-1} peak was caused by stretching of the Fe–O bond.[40] A change is observed in the intensities of absorbance peaks by the introduction of a tiny amount of CQDs. These results indicate that CQDs modify the surface of $CaFe_2O_4$ without affecting it.

4.3 Morphological analysis

The SEM pictures in Fig. 3(a–c) show the shape and crystalline structure of $CaFe_2O_4$ and $CaFe_2O_4$/CQDs materials. Fig. 3(a) shows that $CaFe_2O_4$ has a nanostructure with a diameter of less than 10 nm, which is consistent with the diffraction

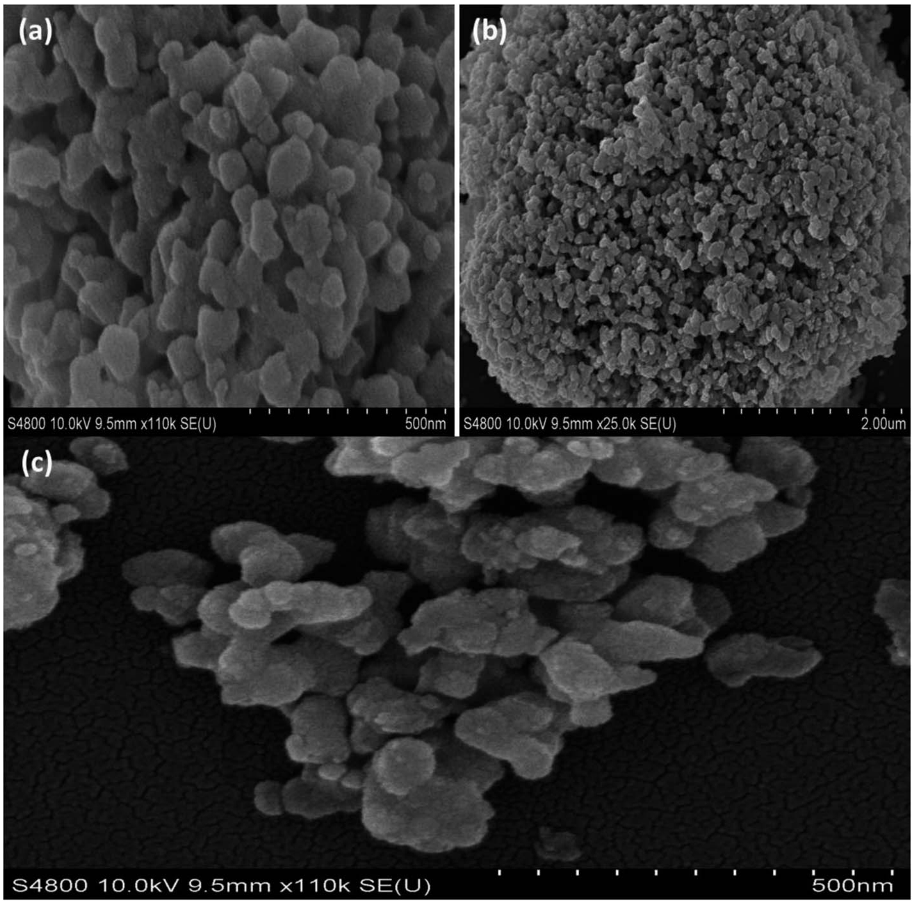

Fig. 3 Scanning electron microscopy (SEM) of the (a and b) $CaFe_2O_4$, (c) $CaFe_2O_4$/CQDs.

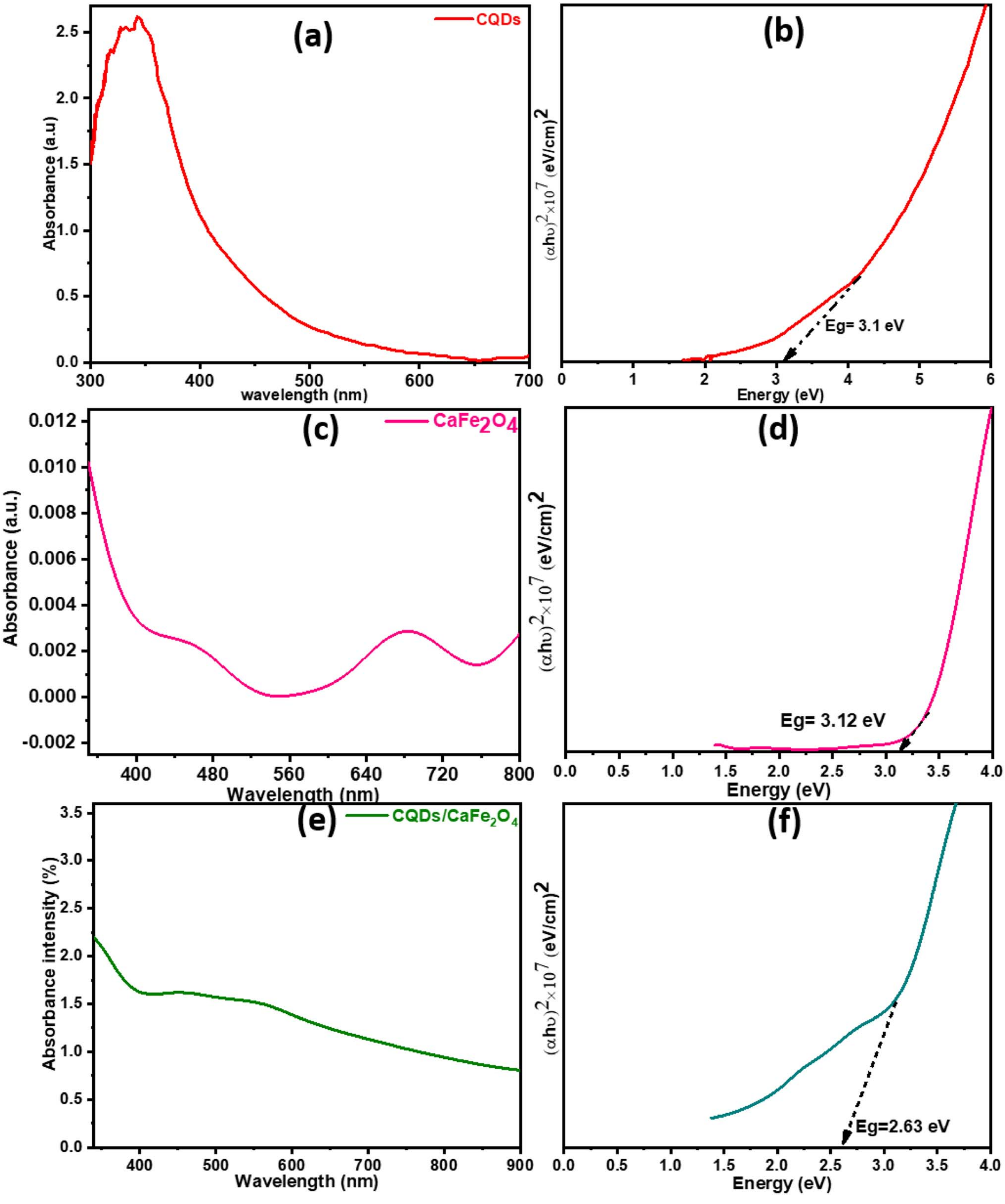

Fig. 4 (a, c and e) Absorption spectra and (b, d and f) Tauc plots of $CaFe_2O_4$, CQDs and $CaFe_2O_4$/CQDs, respectively.

peaks shown in the XRD pattern. $CaFe_2O_4$ retains its original form and size distribution after being treated using 5 nm CQDs (Fig. 3(c)).

4.4 UV-visible spectroscopy

In the UV spectra of CQDs, $CaFe_2O_4$, $CaFe_2O_4$/CQDs (Fig. 4(a–c)), the strong absorption of CQDs in the UV region (450 nm) is depicted in Fig. 4(a), while the Fe^{3+} ions at Td and

Oh coordination sites display charge transfer spectra with multiple peaks at 460 and 682 nm (Fig. 4(b)). The O and Ca^{2+} ions swap electrons when $CaFe_2O_4$ develops in the Td and Oh sites.[41] The UV-vis spectra of $CaFe_2O_4$/CQDs (Fig. 4(b)) revealed the same peaks as of $CaFe_2O_4$ with stronger adsorption. We discovered that CQDs improve the light absorbing capacity, enhancing electron and hole pair generation for a better photocatalytic process. The strength of the CQDs/$CaFe_2O_4$ connection is shown by the intensity of the hump. The bandgap values of the $CaFe_2O_4$ and $CaFe_2O_4$/CQDs nanostructures calculated from $(\alpha h\nu)2$ *vs.* eV were 3.12 and 2.63 eV, respectively, as shown in Fig. 4(c and d).[42] The sensitization effect of CQDs lowered the bandgaps of the nanohybrids, allowing more electron–hole pairs to be formed.

4.5 Photocatalytic activity

Visible-light irradiation was utilized for a photo-reduction method in the experiment. An investigation on the photo-reduction efficiency of these materials against CR dye was carried out. The toxic nature of CR, which is widely used as a dye additive in medicines and textiles, has resulted in a host of environmental issues. Dye drainage into drinking water is the most important consequence of textile dyeing. Hormone imbalance, vomiting, and elevated blood pressure are just a few of the unfavorable side effects that dyes can cause. To keep the ecosystem healthy, the dye must be broken down. The dye and nanocomposite were mixed together to begin the experiment, and CR was adsorbed in 30 min on the surface of the catalysts. Photocatalysis, according to our findings, is responsible for a considerable reduction in CR absorption intensity.

To confirm that environmental light and a photocatalyst cause deterioration, a control experiment was conducted. In the first experiment, the dye solution was irradiated without the addition of the photocatalyst, but in the second experiment, the photocatalyst was introduced, but the light was turned off. Due to dye adsorption on the photocatalyst, which was calibrated prior to the final experiment, a minor decrease in absorbance was noted in both of these tests. In the current investigation, it was determined that deterioration was induced by the presence of photocatalysts and exposure to light. As illustrated in Fig. 5(a–c), the strength of dye and catalyst solution absorption was employed to record photo-reduction utilizing the photocatalysts generated. The catalyst clearly demonstrates the degradation of CR at its specified peak absorption wavelength of 580 nm. The photocatalytic reaction shows degradation as follows: $CaFe_2O_4$ < CQDs < $CaFe_2O_4$/CQDs, as displayed in Fig. 5(a–c). The long-term existence and stability of the dye in an aqueous solution were confirmed by a test with a blank dye. $CaFe_2O_4$/CQDs are more efficient than $CaFe_2O_4$ at 13%, 44%, and 90%, respectively, due to the narrowing of the bandgap. After 140 min, the efficiency of $CaFe_2O_4$/CQDs drops to 10% due to recombination. The photocatalytic degradation rate was calculated using eqn (3) and (4) (ref. 40) given below:

$$C_t = C_0 e^{-kt} \tag{3}$$

$$\ln(C_0/C_t) = kt \tag{4}$$

The starting concentration of dye is denoted by C_0 and that after an interval of time to light exposure is denoted by C_t, while the rate constant is denoted by k. The coefficient of variation (k) can be found on the graph of exposure time (t) *vs.* $\ln(C_0/C_t)$. k values 0.01449 and 0.00659 min^{-1} are found in $CaFe_2O_4$ and $CaFe_2O_4$/CQDs, respectively (Fig. 5(c and d)). The $CaFe_2O_4$/CQDs nanocomposite shows a higher rate constant value than $CaFe_2O_4$, as can be seen in Fig. 5(e).

4.6 Photodegradation mechanism

On the catalyst, photons with energy equal to or greater than the bandgap excite electrons from the valence band (VB) into the conduction band (CB), forming electron (e^-)–hole (h^+) pairs.

$$\mathrm{CaFe_2O_4/CQDs} \xrightarrow{h\nu} \mathrm{e}^- + \mathrm{h}^+ \tag{5}$$

Hydroxyl radicals ($OH^{\bullet}$) are generated when electron donors (H_2O) and OH ions interact with the produced holes. On the other hand, oxygen molecules (O_2) act as electron acceptors while interacting with the electrons in the conduction band. Such interactions within the compounds form hydrogen peroxide (H_2O_2), superoxide radical anions such as hydroxyl radicals (OH^-), and hyperoxyl radicals ($HO^{\bullet}$). The obtained (O^-), ($OH^{\bullet}$), and ($HO^{\bullet}$) radicals react with the Congo red dye, generating aromatic intermediates resulting in a colorless mineralization variation.

$$\mathrm{Dye} + (\mathrm{OH}^{\bullet}), (\mathrm{O_2}^{-}), (\mathrm{H}_2^{:}) \xrightarrow{\text{intermediate}} \text{final product} \tag{6}$$

The photocatalytic destruction of Congo red utilized $CaFe_2O_4$/CQDs nanoparticles. $CaFe_2O_4$/CQDs nanoparticles can be coated with Congo red dye that is dissolved in water and adsorbed onto the positive surface to generate a negative charge.

It is probable that the deionization state of the catalyst has an effect on dye adsorption. When positive holes react with essential hydroxyl ions, oxyl radicals are formed. In alkaline media, the interaction of hydroxyl radicals with positive holes can aid in photodegradation and photocatalytic amplification. The existence of native point defects in $CaFe_2O_4$/CQDs resulted in 90% photocatalytic efficiency. Negatively- and positively-charged OH ions are deposited above and below this threshold on the surfaces of $CaFe_2O_4$/CQDs. When the Congo red surface and the catalyst are charged in different directions, the photocatalytic interaction is improved, increasing efficiency. If a positively charged particle is present on the surface, O_2 can be changed to $O^{\bullet}$. Due to the fact that soaking the holes decreases electron–hole recombination, more OH is produced.

As a result, the photocatalytic activity of both radical ions is enhanced ($O^{\bullet}$ and $OH^{\bullet}$). Congo red undergoes a color shift during photocatalysis. As a result of dye degradation, a paler tone may appear. The presence of light and catalysts both have an effect on photodegradation. Fig. 7(a and b) illustrate two alternative experimental setups for the photocatalytic degradation of a 100 mL aqueous Congo red dye solution: without solar irradiation; with the catalyst exposed to sunlight. After 140 min

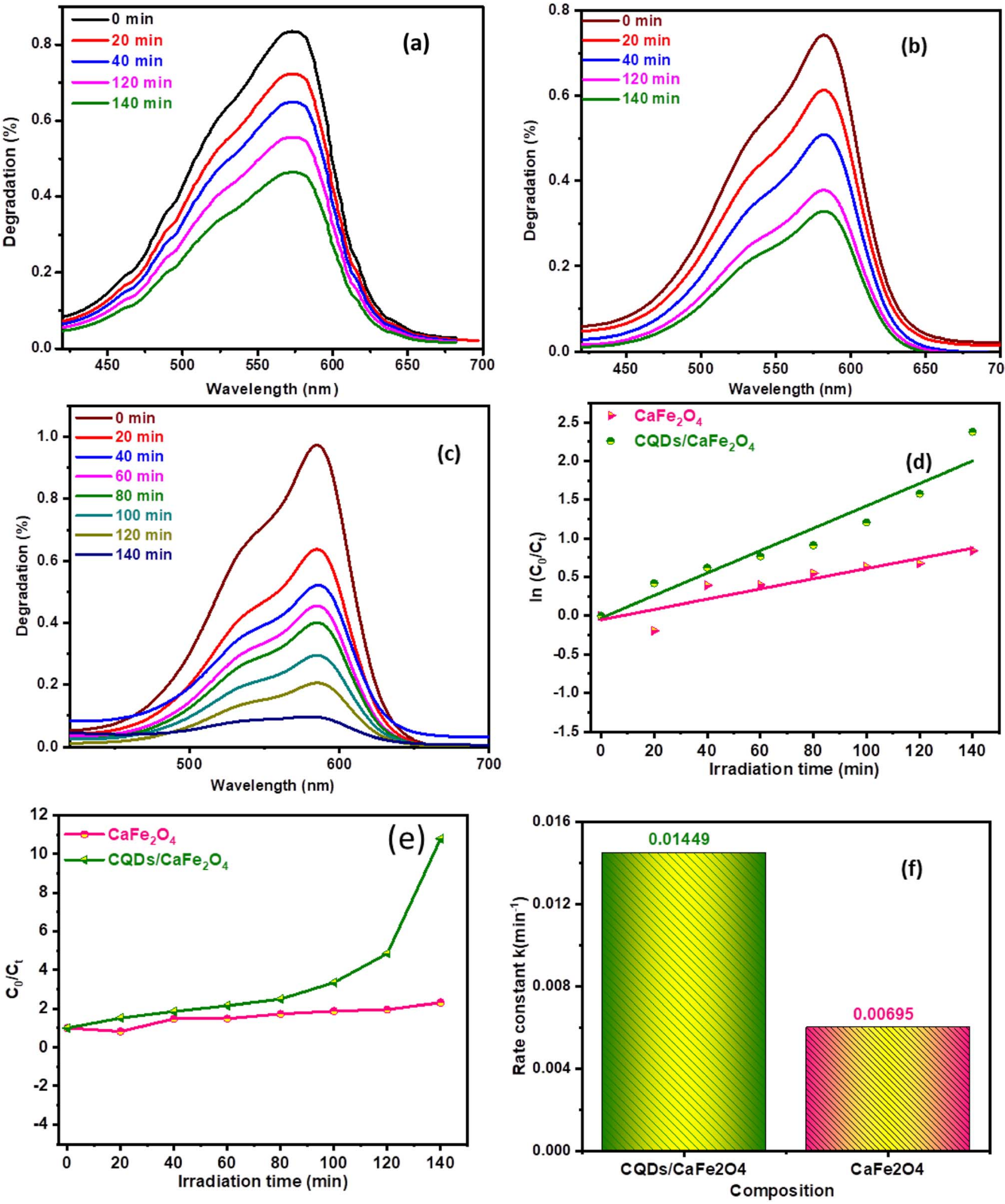

Fig. 5 Variation in absorption spectra of CR dye in the presence of (a) $CaFe_2O_4$, (b) CQDs, (c) $CaFe_2O_4$/CQDs catalysts, (d) plot of C_0/C_t *vs.* irradiation time, (e) rate constant plots, (f) rate constant k (min^{-1}).

in the light, the degradation rate increased to 90%. Despite the fact that magnetic stirring was used for the same duration as the light was present, the degradation of Congo red dye and the $CaFe_2O_4$ mixture was kept to a minimum (13%). When exposed to sunshine, $CaFe_2O_4$/CQDs are certainly responsible for the degeneration of Congo red (curve CR without catalyst but with solar light). A mixture of $CaFe_2O_4$ and CQDs was shown to be an effective nanocomposite for the degradation of Congo red.

When CQDs were added to $CaFe_2O_4$, the photocatalytic activity was greatly boosted. The mechanism of the photodegradation using $CaFe_2O_4$/CQDs is given below,

$$CaFe_2O_4/CQDs + h\upsilon \rightarrow CaFe_2O_4\ (h^+) + CQDs\ (e^-) \quad (7)$$

$$e^- + O_2 \rightarrow O^{\bullet} \quad (8)$$

$$h + OH^- \rightarrow OH^{\bullet} \quad (9)$$

$$O_2 + H_2O \rightarrow HO_2 + OH^- \quad (10)$$

$$HO_2^{\ +} + H_2O \rightarrow OH^{\bullet} + H_2O_2 \quad (11)$$

$$H_2O_2 \rightarrow 2OH^{\bullet} \quad (12)$$

$$CR + OH^{\bullet} \rightarrow \text{Degradation of CR} \quad (13)$$

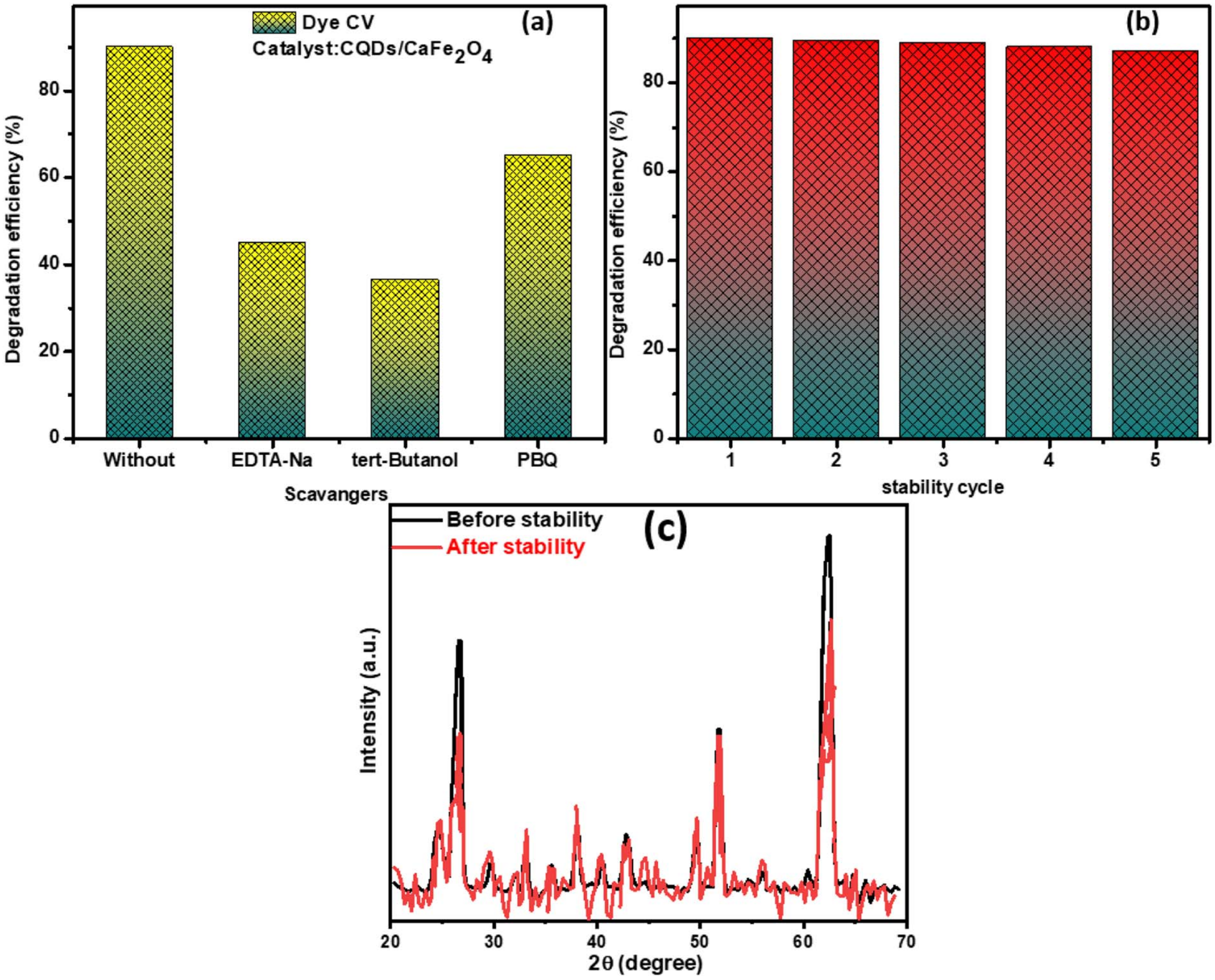

Fig. 6 (a) Scavenger test, (b) cycling stability, and (c) XRD patterns before after stability testing.

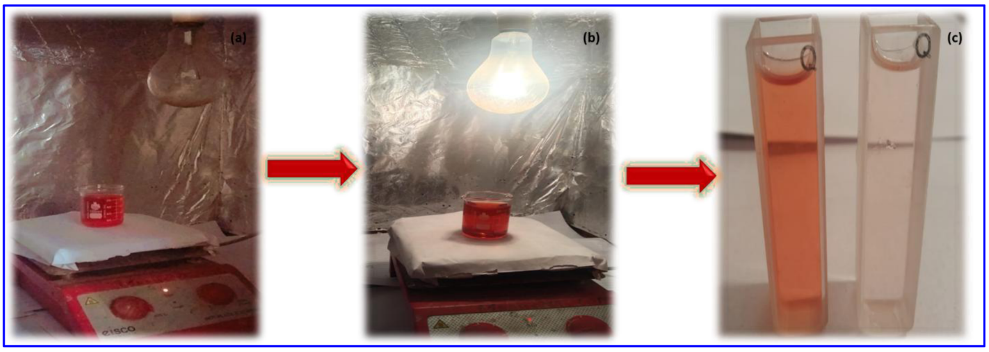

Fig. 7 Experimental setup in the dark (a), in visible light (b), and comparative results (c).

We conducted trapping experiments in order to better understand the catalytic process of $CaFe_2O_4$/CQDs with the aim of reducing the efficiency from 89% to 68%, 45%, and 39% depending on the use of *p*-benzoquinone (a scavenger of O_2), EDTA-2Na (a scavenger of h^+), and tertiary-butanol (a scavenger of OOH), as displayed in Fig. 6(a). In the photocatalytic degradation of CR using the $^{\bullet}OH$ scavenger, with the primary reactants being $^{\bullet}OH$ and the secondary reactants being $^{\bullet}O_2$ and h^+, a significant reduction in photocatalytic efficiency was observed, which could be attributed to the use of the $^{\bullet}OH$ scavenger. The ability of photocatalysts to be reused, as well as their stability over time are essential characteristics. As a consequence, the composite material underwent five cycles in succession. It was later proven to be an efficient photocatalyst, as can be seen in Fig. 6(b). Unfortunately, the efficiency of the composite material diminished marginally after five cycles. In addition, the XRD pattern of the composite material was captured after five successive rounds, as shown in Fig. 6(c), in order to explore the stability of the composite material and determine its strength. All peaks connected to the composite material in the XRD patterns showed a minor drop in intensity, showing that the photocatalyst is stable and may be utilized in the future.

5. Conclusions

In this work, a novel nanocomposite calcium ferrite modified by carbon quantum dots ($CaFe_2O_4$/CQDs) was synthesized by a one-pot hydrothermal method. Schemes for the synthesis of CQDs and $CaFe_2O_4$/CQDs were discussed in detail. The physical, chemical and structural properties of $CaFe_2O_4$/CQDs were studied *via* different characterization techniques. The modification with CQDs reduced the bandgap from 3.12 eV ($CaFe_2O_4$) to 2.63 eV ($CaFe_2O_4$/CQDs). The photocatalytic activity of the nanocomposites against Congo red dye increased up to 90% due to the CQDs. The efficient synthesis method, visible light-driven photocatalytic behaviour, and lower bandgap led to the conclusion that the $CaFe_2O_4$/CQDs nanocomposite is a suitable choice to degrade carcinogenic Congo red dye for environmental remediation.

Conflicts of interest

There are no conflicts of interest to declare.

Acknowledgements

Inam Ur Rehman and Hasan M. Khan appreciate support from Director Institute of Physics, The Islamia University of Bahawalpur. M. A. A. and Muhammad Imran express their appreciation to the Deanship of Scientific Research at King Khalid University, Saudi Arabia, for funding this work through research group program under grant number RGP. 2/370/44. Thamraa Alsharani appreciates the Princess Nourah bint Abdulrahman University Researchers Supporting Project number (PNURSP2023R1), Princess Nourah bint Abdulrahman University, Riyadh, Saudi Arabia.

References

1 H. M. Khan, Z. Mirrani, A. Waheed, J. Ahmad, M. E. Mazhar, M. N. Usmani, I. Syed, S. Bakhtawar, I. Ahmad, W. Abbas, R. Naz, S. Ahmad and M. Mahmood, Synthesis and characterization of rare earth substituted M-type (SR-BA) hexaferrites, *J. Ovonic Res.*, 2020, **16**, 171–192.

2 C. A. Martínez-Huitle and E. Brillas, Decontamination of wastewaters containing synthetic organic dyes by electrochemical methods: a general review, *Appl. Catal., B*, 2009, **87**, 105–145.

3 M. Abdullah, P. John, Z. Ahmad, M. N. Ashiq, S. Manzoor, M. I. Ghori, M. U. Nisa, A. G. Abid, K. Y. Butt and S. Ahmed, Visible-light-driven $ZnO/ZnS/MnO_2$ ternary nanocomposite catalyst: synthesis, characterization and photocatalytic degradation of methylene blue, *Appl. Nanosci.*, 2021, 1–10.

4 S. Manzoor, M. Malana, T. Alshahrani, R. Gohar, W. Khan, M. Najam-ul-Haq, M. Ehsan, A. Shah, M. Ashiq and S. Ahmed, Visible-light-driven zirconium oxide/cadmium sulfide nanocomposite for degradation of textile dyes, *Int. J. Environ. Sci. Technol.*, 2021, 1–10.

5 M. B. Shekardasht, M. H. Givianrad, P. Gharbani, Z. Mirjafary and A. Mehrizad, Preparation of a novel Z-scheme $g\text{-}C_3N_4/RGO/Bi_2Fe_4O_9$ nanophotocatalyst for degradation of Congo Red dye under visible light, *Diamond Relat. Mater.*, 2020, **109**, 108008.

6 W. Shi, C. Hao, Y. Shi, F. Guo and Y. Tang, Effect of different carbon dots positions on the transfer of photo-induced charges in type I heterojunction for significantly enhanced photocatalytic activity, *Sep. Purif. Technol.*, 2023, **304**, 122337.

7 M. M. Tauber, G. M. Gübitz and A. Rehorek, Degradation of azo dyes by oxidative processes–Laccase and ultrasound treatment, *Bioresour. Technol.*, 2008, **99**, 4213–4220.

8 W. Shi, C. Hao, Y. Fu, F. Guo, Y. Tang and X. Yan, Enhancement of synergistic effect photocatalytic/persulfate activation for degradation of antibiotics by the combination of photo-induced electrons and carbon dots, *Chem. Eng. J.*, 2022, **433**, 133741.

9 H. M. Khan, M. U. Islam, Y. Xu, M. Asif Iqbal and I. Ali, Structural and Magnetic Properties of TbZn-Substituted Calcium Barium M-type Nano-structured Hexa-ferrites, *J. Alloys Compd.*, 2014, **589**, 258–262.

10 W. Shi, Y. Liu, W. Sun, Y. Hong, X. Li, X. Lin, F. Guo and J. Shi, Improvement of synergistic effect photocatalytic/peroxymonosulfate activation for degradation of amoxicillin using carbon dots anchored on rod-like $CoFe_2O_4$, *Chin. J. Chem. Eng.*, 2022, **52**, 136–145.

11 M. Zahid, H. M. Khan, M. A. Assiri, M. Imran and S. A. Buzdar, Structural, Morphological, Dielectric, and Magnetic Properties of $Pb_{1-x}Cr_xFe_{12}O_{19}$ M-type Hexaferrites, *Mater. Sci. Eng.: B*, 2022, **280**, 115707.

12 S. Shen, D. Wang, M. Jia, S. Xiao, Z. Tang and J. Yang, Ultrafast and high efficiency photodegradation of dyes under visible light by Au nanocluster-promoted $Zn_{0.5}Cd_{0.5}S$ nanorods, *CrystEngComm*, 2021, **23**, 3288–3296.

13 T. Wang, X. Tang, S. Zhang, J. Zheng, H. Zheng and L. Fang, Roles of functional microbial flocculant in dyeing wastewater treatment: Bridging and adsorption, *J. Hazard. Mater.*, 2020, **384**, 121506.

14 M. Zahid, H. M. Khan, M. Imran, M. A. Assiri, A. U. Rehman and Z. Batool, Enhanced Structural and Dielectric Properties of Calcium and Chromium-Based MM-Type Hexagonal Ferrites with Polyvinyl Alcohol (PVA), *Polym. Compos.*, 2022, **17**, 2250048.

15 H. M. Khan, M. Mustaqeem, Y. F. Chen, M. Junaid, T. A. Saleh, M. N. Akram, A. U. Rehman and N. Lateef, Tuning of structural and dielectric properties of X type hexaferrite through Co and Zn variation, *J. Alloys Compd.*, 2022, **909**, 164529.

16 D. Jager, D. Kupka, M. Vaclavikova, L. Ivanicova and G. Gallios, Degradation of Reactive Black 5 by electrochemical oxidation, *Chemosphere*, 2018, **190**, 405–416.

17 S. Zheng, H. Chen, X. Tong, Z. Wang, J. C. Crittenden and M. Huang, Integration of a Photo-Fenton Reaction and a Membrane Filtration using CS/PAN@ FeOOH/g-C_3N_4Electrospun Nanofibers: Synthesis, Characterization, Self-cleaning Performance and Mechanism, *Appl. Catal., B*, 2021, **281**, 119519.

18 H. M. Khan, M. U. Islam, Y. Xu, M. Asif Iqbal, I. Ali, M. Ishaque and M. A. Khan, Structural, magnetic, and microwave properties of NdZn-substituted $Ca_{0.5}Ba_{0.5}Fe_{12}O_{19}$ hexaferrites, *J. Sol-Gel Sci. Technol.*, 2015, **75**(2), 305–312.

19 M. Zahid, H. M. Khan, A. U. Rehman, A. Waheed, I. Sadiq, E. Mazhar, M. A. Assiri, M. Imran, M. I. U. Rehman and M. Mustaqeem, Structural, morphological, dielectric and magnetic properties of $Ba_{1-x}Cr_xFe_{12}O_{19}$ M type hexaferrites, *Phys. Scr.*, 2021, **96**, 125405.

20 R. E. Adam, G. Pozina, M. Willander and O. Nur, Synthesis of ZnO nanoparticles by co-precipitation method for solar driven photodegradation of Congo red dye at different pH, *Photonics Nanostruct.*, 2018, **32**, 11–18.

21 H. Yuan, W. Shi, J. Lu, J. Wang, Y. Shi, F. Guo and Z. Kang, Dual-channels separated mechanism of photo-generated charges over semiconductor photocatalyst for hydrogen evolution: Interfacial charge transfer and transport dynamics insight, *Chem. Eng. J.*, 2023, **454**, 140442.

22 Z. Xu, W. Shi, Y. Shi, H. Sun, L. Li, F. Guo and H. Wen, Carbon dots as solid-state electron mediator and electron acceptor in S-scheme heterojunction for boosted photocatalytic hydrogen evolution, *Appl. Surf. Sci.*, 2022, **595**, 153482.

23 K. Tezuka, M. Kogure and Y. J. Shan, Photocatalytic degradation of acetic acid on spinel ferrites MFe_2O_4 (M = Mg, Zn, and Cd), *Catal. Commun.*, 2014, **48**, 11–14.

24 B. Paul, B. Bhuyan, D. D. Purkayastha, S. S. Dhar and S. Behera, Facile synthesis of spinel $CuCr_2O_4$ nanoparticles and studies of their photocatalytic activity in degradation of some selected organic dyes, *J. Alloys Compd.*, 2015, **648**, 629–635.

25 J. Lu, Y. Shi, Z. Chen, X. Sun, H. Yuan, F. Guo and W. Shi, Photothermal effect of carbon dots for boosted photothermal-assisted photocatalytic water/seawater splitting into hydrogen, *Chem. Eng. J.*, 2023, **453**, 139834.

26 M. Mujahid, H. M. Khan, Z. Sarwar, K. Ali, M. Shoib, I. Sadiq, X. U. Yongbing, M. Zahid, M. Nadeem, T. Akhtar, R. Anjum and I. U. Rehman, Synthesis and Characterization of Aluminium and Cobalt substituted W type Hexagonal Ferrites, *J. Nanoscope*, 2020, **2**, 2788–7456.

27 H. M. Khan, M. U. Islam, Y. Xu, M. N. Ashiq, I. Ali, M. Asif Iqbal and M. Ishaque, Structural and Magnetic Properties of Pr–Ni Substituted $Ca_{0.5}Ba_{0.5}Fe_{12}O_{19}$ hexa-ferrite Nanoparticles, *Ceram. Int.*, June 2014, **40**(Issue 5), 6487–6493.

28 R. Koutavarapu, C. V. Reddy, K. Syed, K. R. Reddy, T. A. Saleh, D.-Y. Lee, J. Shim and T. M. J. Aminabhavi, Novel Z-scheme Binary Zinc Tungsten Oxide/Nickel Ferrite Nanohybrids for Photocatalytic Reduction of Chromium (Cr (VI)), Photoelectrochemical Water Splitting and Degradation of Toxic Organic Pollutants, *J. Hazard. Mater.*, 2021, **423**, 127044.

29 Z. Jiang, K. Chen, Y. Zhang, Y. Wang, F. Wang, G. Zhang and D. D. Dionysiou, Magnetically recoverable $MgFe_2O_4$/ conjugated polyvinyl chloride derivative nanocomposite with higher visible-light photocatalytic activity for treating Cr (VI)-polluted water, *Sep. Purif. Technol.*, 2020, **236**, 116272.

30 A. Kiani, G. Nabiyouni, S. Masoumi and D. Ghanbari, A novel magnetic $MgFe_2O_4$–$MgTiO_3$ perovskite nanocomposite: Rapid photo-degradation of toxic dyes under visible irradiation, *Composites, Part B*, 2019, **175**, 107080.

31 I. Shakir, P. O. Agboola and S. Haider, Manganese spinel ferrite-reduced graphene oxides nanocomposites for enhanced solar irradiated catalytic studies, *Ceram. Int.*, 2021, **47**, 28367–28376.

32 S. Xiao, A. Fakhri and B. J. Janani, Synthesis of spinel Tin ferrite decorated on Bismuth ferrite nanostructures for synergetic photocatalytic, superior drug delivery, and antibacterial efficiencies, *Surf. Interfaces*, 2021, 101490.

33 J. Hammouche, M. Gaidi, S. Columbus and M. J. Omari, Enhanced Photocatalytic Performance of Zinc Ferrite Nanocomposites for Degrading Methylene Blue: Effect of Nickel Doping Concentration, *J. Inorg. Organomet. Polym. Mater.*, 2021, 1–9.

34 T. Abraham, R. N. Priyanka, S. Joseph, A. R. Chacko and B. Mathew, Fabrication of zirconium ferrite doped Ag_3PO_4 composite for the degradation of refractory pollutants: Visible light assisted Z-scheme insight, *Mater. Sci. Semicond. Process.*, 2021, **130**, 105797.

35 H. Wu, C. Mi, H. Huang, B. Han, J. Li and S. Xu, Solvothermal synthesis of green-fluorescent carbon nanoparticles and their application, *J. Lumin.*, 2012, **132**, 1603–1607.

36 S. Altaf, H. Ajaz, M. Imran, A. Ul-Hamid, M. Naz, M. Aqeel, A. Shahzadi, A. Shahbaz and M. Ikram, Synthesis and characterization of binary selenides of transition metals to investigate its photocatalytic, antimicrobial and anticancer efficacy, *Appl. Nanosci.*, 2020, **10**, 2113–2127.

37 M. H. Khan, S. Mumtaz, A. Waheed, J. Ahmad, M. E. Mazhar, W. Abbas, I. Khan, M. N. Usmani, S. Bakhtawar, A. Javed, G. A. Ashraf, S. Ahmad, R. Naz and S. Ahmad, *J. Ovonic Res.*, 2021, **02**(17), 165–173.

38 M. Goodarzi, S. Joukar, D. Ghanbari and K. Hedayati, $CaFe_2O_4$–ZnO magnetic nanostructures: photo-degradation of toxic azo-dyes under UV irradiation, *J. Mater. Sci.: Mater. Electron.*, 2017, **28**, 12823–12838.

39 N. Sulaiman, M. Ghazali, J. Yunas, A. Rajabi, B. Majlis and M. Razali, Synthesis and characterization of $CaFe_2O_4$ nanoparticles *via* co-precipitation and auto-combustion methods, *Ceram. Int.*, 2018, **44**, 46–50.

40 B. Smith, *Infrared spectral interpretation: a systematic approach*, CRC Press, 2018.

41 M. Nadeem and H. M. Khan, *et.al.* , Structural, dielectric, and magnetic properties of $CaBaCo_{2\text{-}x}Zn_xNd_yFe_{12\text{-}y}O_{22}$ Y-type hexaferrites, *J. Mater. Sci: Mater. Electron.*, 2022, **33**, 6294–6306.

42 T. Munawar, M. S. Nadeem, F. Mukhtar, M. Hasan, K. Mahmood, M. Arshad, A. Hussain, A. Ali, M. S. Saif and F. Iqbal, Rare earth metal co-doped $Zn_{0\cdot 9}La_0$. 0.5M_0. 0.5O (M= Yb, Sm, Nd) nanocrystals; energy gap tailoring, structural, photocatalytic and antibacterial studies, *Mater. Sci. Semicond. Process.*, 2021, **122**, 105485.